

NACA RM L50G17a

7203

NACA

TECH LIBRARY KAFB, NM
0143817

RESEARCH MEMORANDUM

TRANSONIC FLIGHT TESTS TO COMPARE THE ZERO-LIFT DRAG
OF UNDERSLUNG AND SYMMETRICAL NACELLES VARIED
CHORDWISE AT 40 PERCENT SEMISPAN OF
A 45° SWEEPBACK, TAPERED WING

By William B. Pepper, Jr., and Sherwood Hoffman

Langley Aeronautical Laboratory
Langley Air Force Base, Va.

CLASSIFIED DOCUMENT

Information affecting the National Defense of the United States within the
meaning of the Espionage Laws, Title 18, United States Code, Chapter 11, is hereby
transmitted in confidence and its transmission or the revelation of its contents in any
manner to an unauthorized person is prohibited by law.
Information so classified may be imparted only to those personnel in the Federal Government and its services of the United
States, appropriate civilian officers and employees of the Federal Government, and to United States citizens of known loyalty and discretion who, in the interest
therein, and to United States citizens of known loyalty and discretion who, in the interest

**NATIONAL ADVISORY COMMITTEE
FOR AERONAUTICS**

WASHINGTON

October 25, 1950

319.98/13

Classification cancelled (or changed to Unclassified)

By Authority of Nass. Fed. Pub. Announcement #161
(OFFICER AUTHORIZED TO CHANGE)

By.....
NAME AB. 25 May 56
NK

(GRADE OF OFFICER MAKING CHANGE)

6 Apr. 61
DATE



0143817

NACA RM L50G17a

NATIONAL ADVISORY COMMITTEE FOR AERONAUTICS

RESEARCH MEMORANDUM

TRANSONIC FLIGHT TESTS TO COMPARE THE ZERO-LIFT DRAG
OF UNDERSLUNG AND SYMMETRICAL NACELLES VARIED

CHORDWISE AT 40 PERCENT SEMISPAN OF

A 45° SWEEPBACK, TAPERED WING

By William B. Pepper, Jr., and Sherwood Hoffman

SUMMARY

Rocket-powered models were flown at transonic speeds to determine the effect of nacelle location on the zero-lift drag. Nacelles of fineness ratio 9.66 were mounted in underslung and symmetrical (midwing) positions along the wing chord at 40 percent of the semispan. The noses of the nacelles were located at four chordwise stations equivalent to 0.35, 0.50, 0.76, and 1.20 wing chords ahead of the wing leading edge at 40 percent wing semispan. The wing had a sweepback angle of 45° along the quarter-chord line, an aspect ratio of 6.0, a taper ratio equal to 0.6, and an NACA 65A009 airfoil section in the free-stream direction. The fuselage fineness ratio was 10.0.

Results from flight tests showed that no unfavorable interference effects were evident for either underslung or symmetrical nacelle positions at Mach numbers between 0.80 and 0.93. At a Mach number of 1.0 large unfavorable interference effects were present and caused the experimental nacelle drag coefficients to be from 85 percent to 285 percent higher than the value estimated for the nacelle without interference. Nacelles mounted symmetrically on the wing generally had lower drag coefficients than nacelles located in underslung positions at Mach numbers from 0.95 to 1.20. The symmetrically mounted nacelles located in rear positions at the 35- and 50-percent-chord positions gave the lowest drag, and the underslung location at the 76-percent-chord location had the highest drag. The addition of nacelles to the wings of the models, independent of their chordwise location at 40 percent of the semispan, reduced the Mach number at which the transonic drag rise of the total configuration occurred by 0.03 to 0.07.

INTRODUCTION

As part of a general transonic research program of the National Advisory Committee for Aeronautics to determine the aerodynamic properties of promising configurations, rocket-propelled models were tested in free flight to determine the variations of zero-lift drag coefficient for a medium-size bomber configuration with nacelles in various positions on the wings.

Up to the present time investigations of wing-body-nacelle interference at transonic speeds have been confined to fighter models with low-aspect-ratio wings. Subsonic data on wing-body-nacelle interference effects are available for both low- and high-aspect-ratio-wing aircraft; however, there is a lack of information for medium bomber configurations with high-aspect-ratio wings throughout the transonic speed range.

In order to carry out this investigation a wing-body test configuration with a low drag coefficient and a high force break Mach number well above 0.9 was desired. The wing selected, having a sweepback angle of 45° and an aspect ratio of 6, appears promising for high-speed bomber applications. A thickness ratio of 9 percent was believed adequate to insure that the wing would be structurally applicable to a high-speed bomber and also maintain a force break Mach number above 0.9.

A suitable low-drag fuselage was based on the transonic fuselage developed in free-fall tests by the NACA. This body has low subsonic drag and a force break Mach number above 0.9.

The nacelles adopted for the investigation were designed to house an axial-flow turbojet with thrust augmentation by afterburning. This space requirement results in a nacelle having a fineness ratio which is compatible with low drag. Since the primary purpose of the first phase of this investigation is to explore various chordwise locations for symmetrical and underslung wing nacelles, it was desired to simplify the tests by conducting the present investigation without air flow through the nacelles. Accordingly, a nose fairing was adapted which fair the air inlet of the nacelle to a pointed nose, making it a solid nacelle. However, the basic lines of the nose are designed to accommodate NACA l-series inlets with critical Mach numbers above $M = 0.9$.

Tests of the resulting configuration yielded curves of drag-coefficient variations for models with and without nacelles, nacelle-plus-interference drag coefficients for various nacelle locations, and nacelle base-drag and base-pressure variations over a continuous Mach number range of $M = 0.8$ to $M = 1.25$. The Reynolds number range of the tests is comparable to that of a full-scale bomber flying at 60,000 feet.

SYMBOLS

A	aspect ratio (b^2/S_W)
a	longitudinal acceleration, feet per second per second
b	wing span, feet
C_D	total drag coefficient, based on S_W
C_{DB}	nacelle base-pressure drag coefficient, based on S_F
C_{DN}	drag coefficient for nacelle plus interference, based on S_F
C_{PB}	base-pressure coefficient $\left(\frac{P_B - P}{q}\right)$
c	wing chord at the 40-percent station, inches
e	distance between wing leading edge and nacelle inlet, inches
g	acceleration due to gravity, 32.2 feet per second per second
M	Mach number (V/V_S)
p	free-stream static pressure, pounds per square foot
P_B	nacelle base pressure, pounds per square foot
q	free-stream dynamic pressure, pounds per square foot $\left(\frac{\gamma}{2} \rho M^2\right)$
R	Reynolds number per foot
S_B	nacelle base area, square feet
S_F	frontal area of one nacelle, square feet
S_W	total wing plan-form area, square feet
V	velocity along flight path, feet per second

V_S	speed of sound, feet per second
W	model weight after burnout, pounds
γ	ratio of specific heats, 1.4 for air; or flight-path angle
x	station, inches
y	ordinate, inches

MODELS

Details and dimensions of the wing-body-fin combination, the solid nacelle, and the nacelle reference body are given in figures 1 and 2 and tables I to III. Photographs showing the general arrangements of the models flown are presented as figure 3.

The transonic fuselage, described in reference 1, was reduced from a fineness ratio of 12 to 10 by cutting off the rear one-sixth of the body. In order to fit a 3.25-inch Mk. 7 aircraft rocket motor into this body, the rear 28 percent of the modified body was enlarged. The fuselage was constructed from wood and had an aluminum nose. The frontal area of the fuselage was equal to 0.242 square foot.

The leading edge of the wing intersected the fuselage at the maximum diameter. This wing had a sweepback angle of 45° along the quarter-chord line, an aspect ratio of 6.0 based on total wing area of 3.878 square feet (including area in the body), a taper ratio equal to 0.6, and an NACA 65A009 airfoil section in the free-stream direction. This wing configuration was the same as that used in reference 2. The ratio of total wing plan-form area to the fuselage frontal area was 16.0. Sheet steel inlays, 0.04 inch thick, were imbedded near the upper and lower surfaces of the wooden wing. The steel strengthened the wing and served as an antenna for the NACA two-channel radio telemeter.

The nacelles were bodies of revolution constructed of wood having a fineness ratio of 9.66 and a frontal area of 0.034 square foot. Each nacelle used for this investigation was designed to have an NACA 1-50-250 nose-inlet profile (based on data in reference 3), a cylindrical mid-section, and an afterbody of NACA 111 proportions (reference 4). For the present investigation a conical lofted nose plug (reference 5) was used to close off the nacelle inlet. The dimensioning system used to define the chordwise location of the nacelles refers to the distance

of the nacelle inlet ahead of the wing leading edge at the 40-percent-semispan-wing station. The chordwise locations expressed in percent of wing chord were 35, 50, 76, and 120 percent.

Two vertical positions were tested. The symmetrical or midwing position had the nacelle center line in the wing plane. For the underslung positions (fig. 3(c)), the nacelle center lines remained parallel to the wing chord plane and were displaced on opposite sides of the wing plane. This asymmetric arrangement was used so that any trim change would produce roll and the model would fly at essentially zero lift. Tracking photographs of the models in flight, however, revealed no significant roll or pitch.

Cross-sectional views of the nacelle and of the wing-nacelle intersection taken through the nacelle center line are shown in figures 2(a) and 2(b). No filleting was employed at the nacelle-wing juncture.

Two vertical aluminum fins were used to stabilize the model directionally. No fins were required in the horizontal plane because the sweptback wing was located far enough rearward on the fuselage to stabilize the model in this plane (fig. 1). The leading edges of the fins were swept back 45° and the fins were 0.091 inch thick. The exposed fin plan-form area for two fins equaled 0.468 square foot.

TESTS AND MEASUREMENTS

Ten rocket-propelled zero-lift models were tested at the Langley Pilotless Aircraft Research Station, Wallops Island, Va. Three identical models without nacelles were flown to find the basic drag of the wing-body-fin combination as accurately as possible and the scatter of experimental values that would exist for subsequent models. On the remaining seven models, underslung and symmetrically mounted nacelles were varied along the chord at 40 percent of the wing semispan. These models are classified according to nacelle position in figure 2.

Each model was propelled by a two-stage rocket system and launched from a rail launcher (fig. 3(a)). The first stage consisted of a 5-inch, lightweight, high-velocity aircraft rocket motor that served to accelerate the model from zero velocity to high subsonic speeds. For the second stage, a 3.25-inch Mk. 7 aircraft rocket motor was installed in the fuselage to accelerate the model to supersonic speeds. Tracking instrumentation consisting of a CW Doppler velocimeter and an NACA modified SCR584 tracking unit was used to determine the flight path and deceleration during the coasting flight. A survey of atmospheric conditions at the time of each launching was made through radiosonde measurements from

an ascending balloon. Nacelle base-pressure variations for model J were obtained through an orifice 3/16 inch in diameter located at the center of the base and by use of the NACA telemetering system.

The values of drag coefficient, based on total wing plan-form area for each model, were calculated for flight conditions by use of the formula

$$C_D = - \frac{W}{qgS_W} (a + g \sin \gamma)$$

The difference in drag coefficients of models with nacelles and without nacelles is defined as nacelle-plus-interference drag. This coefficient, based on nacelle frontal area, is

$$C_{DN} = (C_{D_{\text{nacelles on}}} - C_{D_{\text{nacelles off}}}) \frac{S_W}{2S_F}$$

Base pressures were converted to base drag coefficients, based on nacelle frontal area, through the relation

$$C_{DB} = \frac{(p_B - p)}{q} \frac{S_B}{S_F}$$

The Mach number was determined from the velocity of each model and the speed of sound at altitude from corresponding radiosonde records.

RESULTS AND DISCUSSION

Flight tests of the models covered a Reynolds number range from 4.6×10^6 per foot at $M = 0.8$ to 9.3×10^6 per foot at $M = 1.3$, as shown in figure 4. Drag coefficients obtained from the tests are shown in figures 5 to 7. These figures permit a comparison of total drag, nacelle-plus-interference drag, and interference drag coefficients for the various nacelle positions at zero lift.

The nacelle-plus-interference drag coefficient C_{DN} is obtained by taking the difference in drag of models with and without nacelles. Since this drag results from the subtraction of two relatively large values, a large error could be encountered. Therefore, three models without nacelles were flown to determine the scatter in the data for identical models. The faired curves for the three models, based on total wing plan-form area

of 3.878 square feet, are shown in figure 5 and are compared in order to determine the experimental error in the test results. The deviation of the faired curves indicates that the errors to be expected are of the order of ± 0.0004 . From this value, the errors in the nacelle-plus-interference drag coefficients would be expected to be ± 0.023 (based on nacelle frontal area). Photographs of the models in flight showed that there was no appreciable roll due to the underslung nacelle locations.

Curves showing the variation of total drag and nacelle-plus-interference drag for the models through the test Mach number range are given for symmetrical nacelles in figures 6(a) to 6(d) and for underslung nacelles in figures 6(e) to 6(g). The curve for the model with nacelles off is the average of the faired curves in figure 5. The nacelle-plus-interference drag is compared with the drag of a body of revolution having the same fineness ratio and a shape similar to that of the nacelle. The drag of this body is referred to as the drag of an isolated nacelle or an unmounted nacelle not subject to interference effects. From a consideration of experimental and theoretical data, the variation of C_{DN} was estimated by adding the drag coefficients of a parabolic nose and a boattail from two different models (from reference 6) and the drag coefficient of a cylindrical section having a friction coefficient of 0.002. A comparison of the nacelle and the resulting reference body is shown in figure 2(a). The curve for the isolated nacelle drag is believed to be of sufficient accuracy to indicate the nacelle interference effects.

In order to compare the incremental nacelle drags, a composite chart for the four symmetrical positions tested is shown in figure 7(a). For the nacelles mounted symmetrically, a large difference in the drag exists between the forward and rearward positions. The values of the drag of the rear positions F and G are from 20 to 50 percent lower than the values of the drag of the forward positions D and E. It may be seen in figure 7(a) that regions of favorable wing-nacelle-body interference are indicated below approximately $M = 0.93$.

Curves showing the incremental nacelle drag coefficients for the three underslung nacelle positions are presented in figure 7(b). The underslung positions experience no unfavorable interference effects up to approximately $M = 0.93$, which is comparable to results found for the symmetrical positions. The drag of the underslung nacelles is generally higher than the drag of symmetrically mounted nacelles. There is a very abrupt rise in the drag of the underslung nacelles starting at approximately $M = 0.93$ and reaching a maximum at $M = 0.98$. The values of the drag of the symmetrical nacelles shown in figure 7(a) rise to a peak at a higher Mach number near $M = 1.01$. The 76-percent location, curve J, has the highest drag of the underslung as well as the symmetrical positions.

Figures 7(a) and 7(b) emphasize that the existence of unfavorable interference effects is most pronounced at a Mach number near $M = 1.0$ for the configuration tested. The unfavorable interference becomes less for Mach numbers less than or $M = 1.0$. At a Mach number

of 1.0 the increase in nacelle drag coefficient due to unfavorable interference varies from 85 percent to 285 percent of the drag coefficient estimated for the isolated nacelle.

In general, it may be seen that the addition of nacelles on the wing at the 40-percent-semispan station, independent of location, reduces the drag rise Mach number by 0.03 to 0.07.

The variation of nacelle base-pressure coefficient for model J with the underslung nacelle position, which has the most unfavorable interference drag, is presented for the test Mach number range in figure 8. The accuracy of the base-pressure coefficient varies from ± 0.038 at subsonic speeds to ± 0.013 at supersonic speeds. A pressure greater than atmospheric acted on the nacelle base up to $M = 0.98$. The gradual increase and sudden drop in base pressure at $M = 0.98$ may indicate the movement of a shock wave to the rear of the nacelle base. The drag resulting from this base pressure is shown in the lower part of figure 6(f). From the magnitude of the base-drag coefficients, it is apparent that the base drag had little effect on the nacelle-plus-interference drag at supersonic speeds; however, the positive base pressure may contribute appreciably to reducing the nacelle drag at high subsonic speeds.

In order to study more generally the effect of nacelle position on the incremental nacelle drag, a cross plot of figure 7 for six Mach numbers is presented in figures 9(a) to 9(f). Each figure shows the nacelle-plus-interference drag coefficient for both underslung and symmetrical positions with varying chordwise location of the nacelle. The lengths e and c defined in figure 2 are measured along the nacelle center line at 40 percent of the wing semispan. The level of drag expected, if there were no interference, is shown as a dash line called "Isolated nacelle."

Figure 9(a) shows that at a Mach number of 0.9 the underslung positions have low drag coefficients which compare favorably with the symmetrical locations despite the fact that there were acute angles between the wing and nacelle due to the absence of filleting on any of the models. The indication that favorable interference effects exist for the 35-percent symmetrical position is supported by similar favorable effects found in reference 7. At $M = 0.95$ (fig. 9(b)) the 35-percent symmetrical position has the lowest drag coefficient. The variations in drag at $M = 1.0$ are shown in figure 9(c). The trend shows that the symmetrical positions have lower drag than the corresponding underslung positions. Nacelles at the 35- and 50-percent symmetrical positions have approximately equal drag, but a large rise in drag is experienced in moving the nacelle forward from the 50- to the 76-percent station. The same general trends are shown at $M = 1.05$ (fig. 9(d)) and $M = 1.15$ (fig. 9(e)). The 76-percent position has the largest drag increment for all locations

tested. The highest test Mach number of 1.25 (shown in fig. 9(f)) indicates that no unfavorable interference was present for the 35-percent and 50-percent locations.

From these tests it is apparent that the drag increment associated with adding nacelles to a wing-body combination is largely dependent upon the nacelle location.

CONCLUSIONS

Swept-wing-nacelle interference effects have been obtained experimentally by transonic flight tests at zero lift. Underslung and symmetrically mounted solid nacelles were varied in a direction parallel to the free stream along the wing chord at the 40-percent station of a 45° sweptback wing. The following effects were noted:

1. No unfavorable interference effects were evident for either underslung or symmetrical nacelles at Mach numbers between 0.80 and 0.93.
2. The highest nacelle drag coefficients measured throughout the test Mach number range occurred near $M = 1.0$. At this Mach number the nacelle drag coefficients were from 85 percent to 285 percent higher than the drag coefficient estimated for the nacelle without interference.
3. Nacelles mounted symmetrically on the wing generally had lower drag coefficients than nacelles located in underslung positions at Mach numbers from 0.95 to 1.20.
4. The symmetrically mounted nacelles located at rearward positions at the 35- and 50-percent-chord stations gave the lowest drag.
5. The highest drag for the underslung nacelle positions was found to be the 76-percent-chord station, and moving the nacelle forward or rearward from this position lowered the drag.
6. The addition of nacelles on the wings of the models, independent of their chordwise location at 40 percent of the semispan, reduced the Mach number at which the transonic drag rise of the total configuration occurred by 0.03 to 0.07.

Langley Aeronautical Laboratory
National Advisory Committee for Aeronautics
Langley Air Force Base, Va.

REFERENCES

1. Thompson, Jim Rogers: Measurements of the Drag and Pressure Distribution on a Body of Revolution throughout Transition from Subsonic to Supersonic Speeds. NACA RM L9J27, 1950.
2. Spreemann, Kenneth P., Morrison, William D., Jr., and Pasteur, Thomas B., Jr.: Aerodynamic Characteristics of a Wing with Quarter-Chord Line Swept Back 45° , Aspect Ratio 6, Taper Ratio 0.6, and NACA 65A009 Airfoil Section. Transonic-Bump Method. NACA RM L50B03a, 1950.
3. Baals, Donald D., Smith, Norman F., and Wright, John B.: The Development and Application of High-Critical-Speed Nose Inlets. NACA Rep. 920, 1948.
4. Abbott, Ira H.: Fuselage-Drag Tests in the Variable-Density Wind Tunnel: Streamline Bodies of Revolution, Fineness Ratio of 5. NACA TN 614, 1937.
5. Dannenberg, Robert E.: The Development of Jet-Engine Nacelles for a High-Speed Bomber Design. NACA RM A7D10, 1947.
6. Hart, Roger G., and Katz, Ellis R.: Flight Investigations at High-Subsonic, Transonic, and Supersonic Speeds to Determine Zero-Lift Drag of Fin-Stabilized Bodies of Revolution Having Fineness Ratios of 12.5, 8.91, and 6.04 and Varying Positions of Maximum Diameter. NACA RM L9I30, 1949.
7. Welsh, Clement J., and Morrow, John D.: Effect of Wing-Tank Location on the Drag and Trim of a Swept-Wing Model as Measured in Flight at Transonic Speeds. NACA RM L50A19, 1950.

TABLE I
FUSELAGE COORDINATES

x (in.)	y (in.)
0	0
.4	.185
.6	.238
1.0	.342
2.0	.578
4.0	.964
6.0	1.290
8.0	1.577
12.0	2.074
16.0	2.472
20.0	2.772
24.0	2.993
28.0	3.146
32.0	3.250
36.0	3.314
40.0	3.334
44.0	3.304
48.0	3.219
52.0	3.037
56.0	2.849
60.0	2.661
64.0	2.474
66.7	2.347



~~CONFIDENTIAL~~

TABLE II
 COORDINATES OF THE NACA 65A009 AIRFOIL

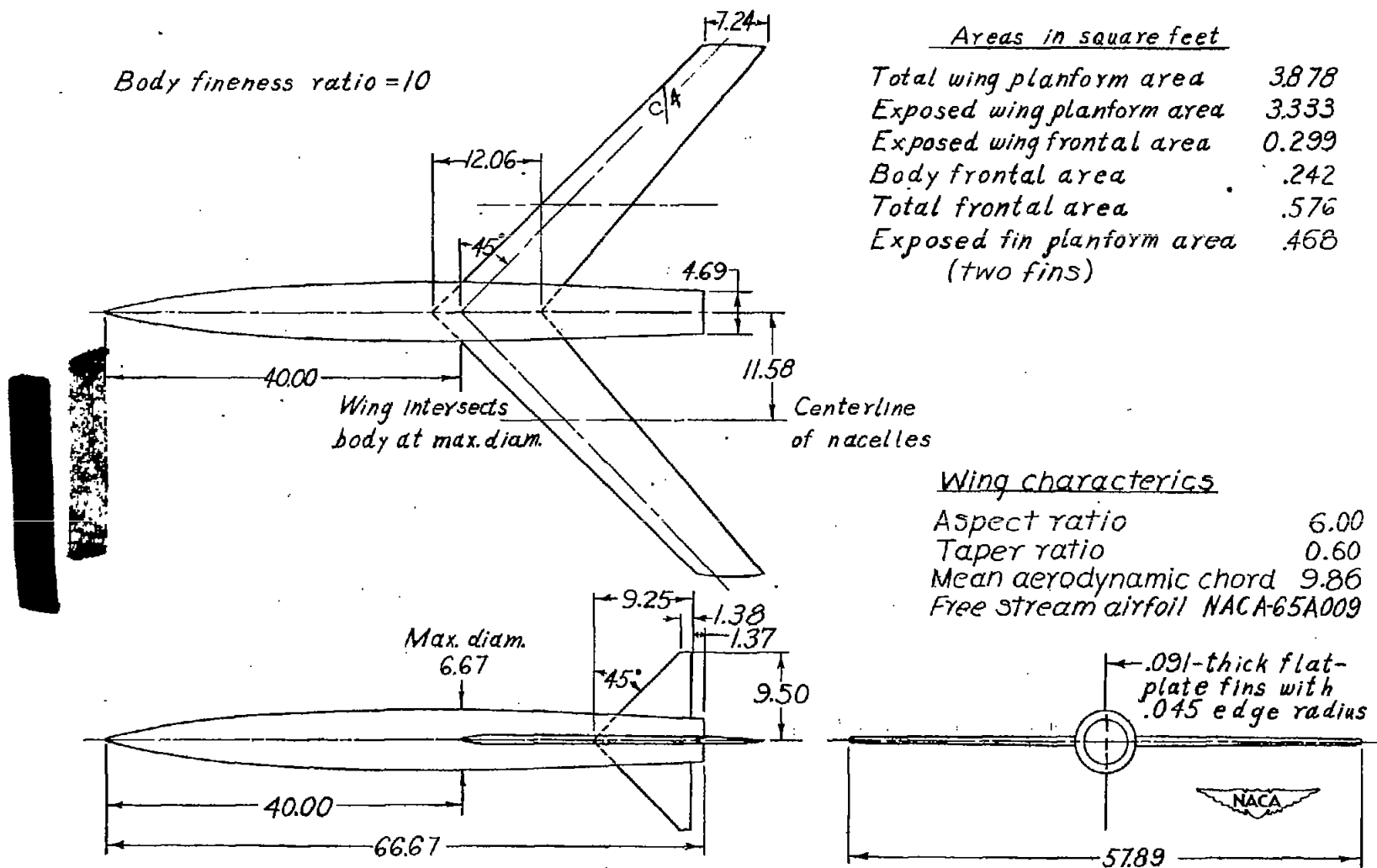
x/c (percent)	y/c (percent)
0	0
.5	.688
.75	.835
1.25	1.065
2.5	1.460
5.0	1.964
7.5	2.385
10.0	2.736
15.0	3.292
20.0	3.714
25.0	4.036
30.0	4.268
35.0	4.421
40.0	4.495
45.0	4.485
50.0	4.377
55.0	4.169
60.0	3.874
65.0	3.509
70.0	3.089
75.0	2.620
80.0	2.117
85.0	1.594
90.0	1.069
95.0	.544
100.0	.019

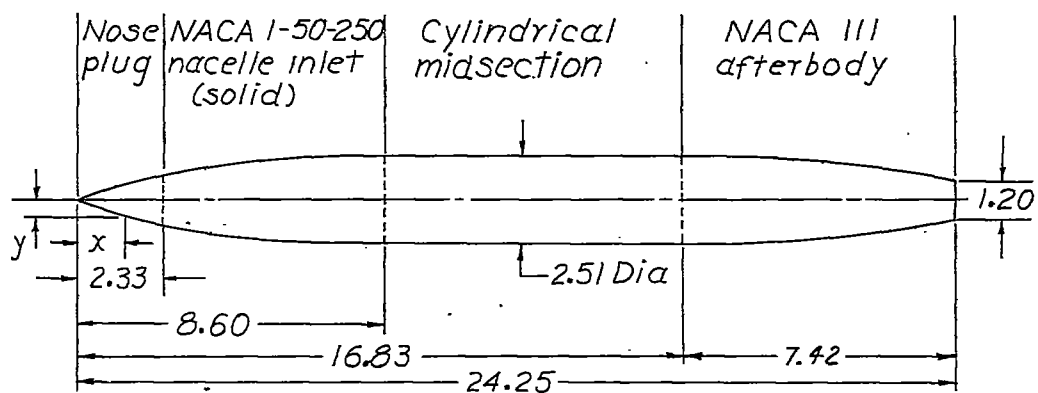
~~CONFIDENTIAL~~

TABLE III
COORDINATES FOR SOLID NACELLE

x (in.)	y (in.)
0	0
.100	.070
.330	.169
.830	.336
1.330	.489
1.830	.622
2.330	.747
2.580	.800
2.958	.876
3.585	.974
4.840	1.105
6.095	1.190
7.350	1.240
8.605	1.255
16.830	1.255
17.872	1.237
18.913	1.195
19.955	1.127
20.996	1.029
22.038	.909
23.079	.768
24.121	.616
24.250	.598

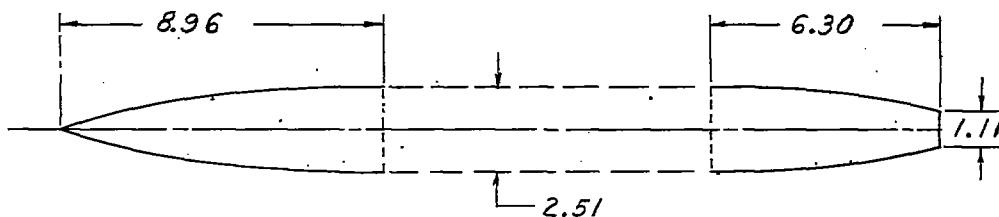






Nacelle frontal area = 0.034 sq ft
 Nacelle fineness ratio = 9.66

Nacelle



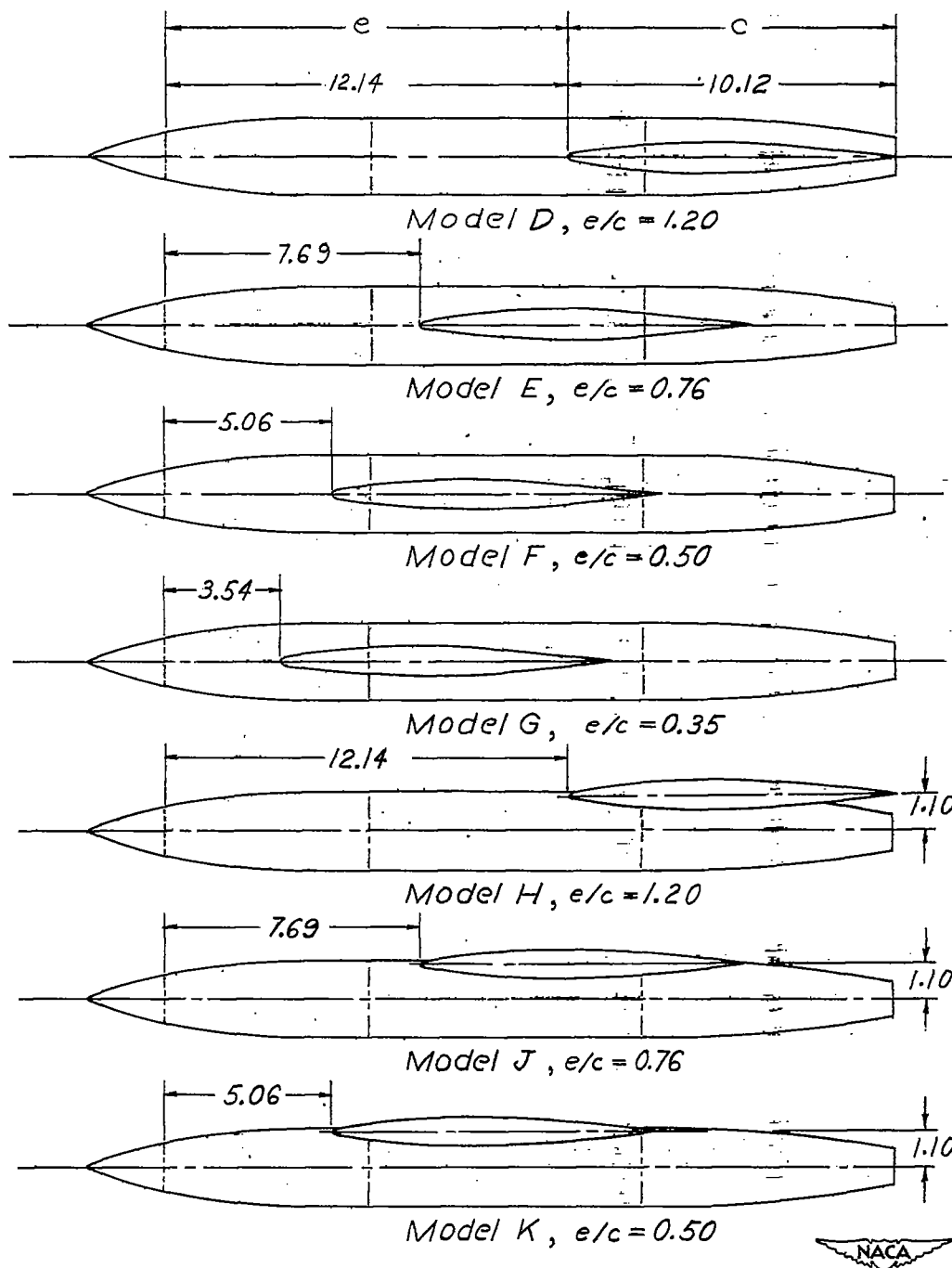
Isolated Nacelle
 Drag reference body



(a) Comparison of nacelle and isolated nacelle.

Figure 2.- Dimensions and arrangement of nacelles. All dimensions are in inches.

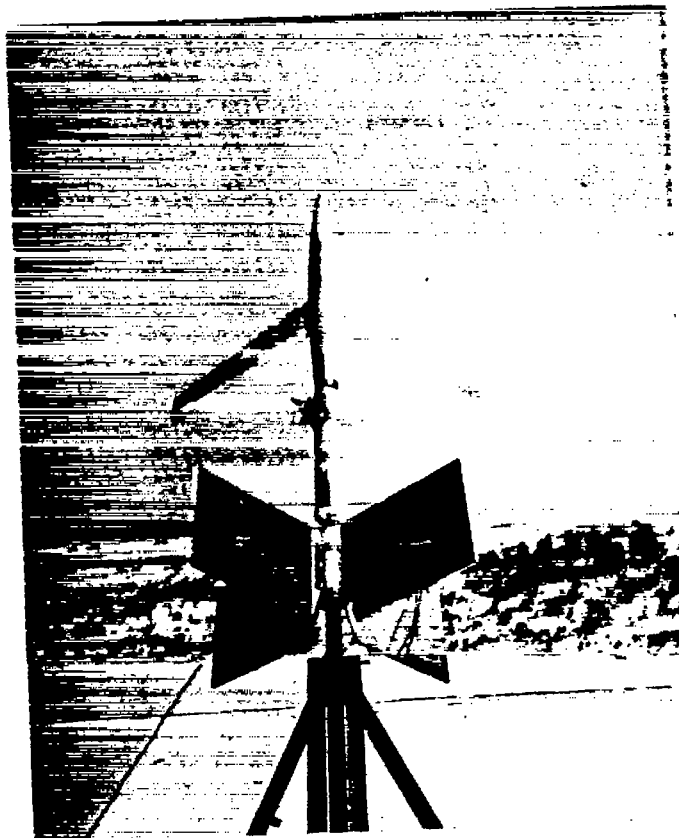
CONFIDENTIAL



(b) Nacelle location on wing chord at 40 percent semispan.

Figure 2.- Concluded.

CONFIDENTIAL

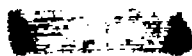
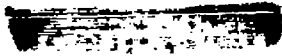


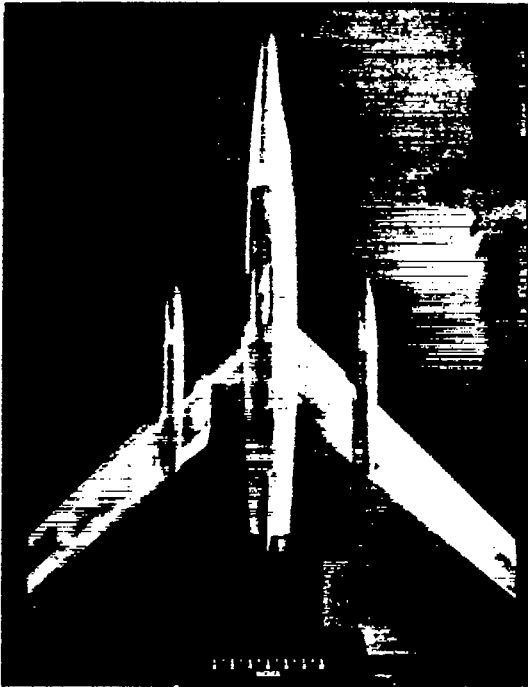
Models A, B, C

NACA
L-64912

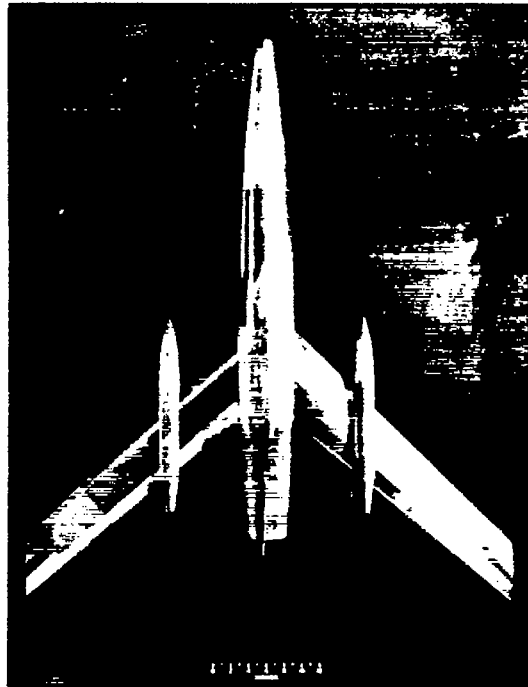
(a) Test model without nacelles. Method of launching and boosting of models at test area.

Figure 3.- General arrangement of test models.

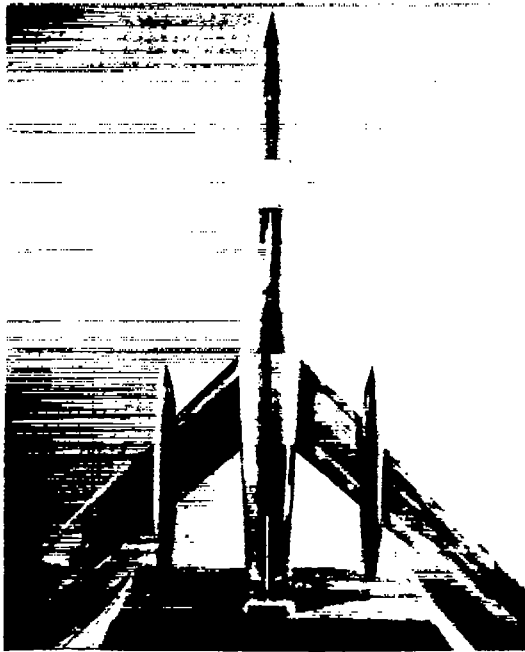




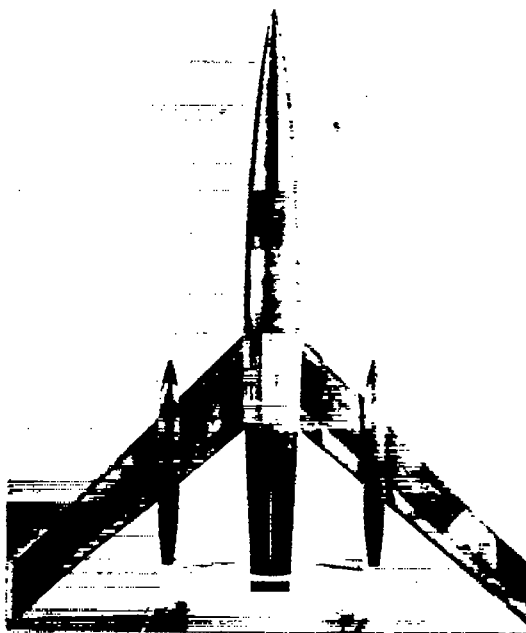
Model D, $\frac{e}{c} = 1.20$.



Model E, $\frac{e}{c} = 0.76$.



Model F, $\frac{e}{c} = 0.50$.



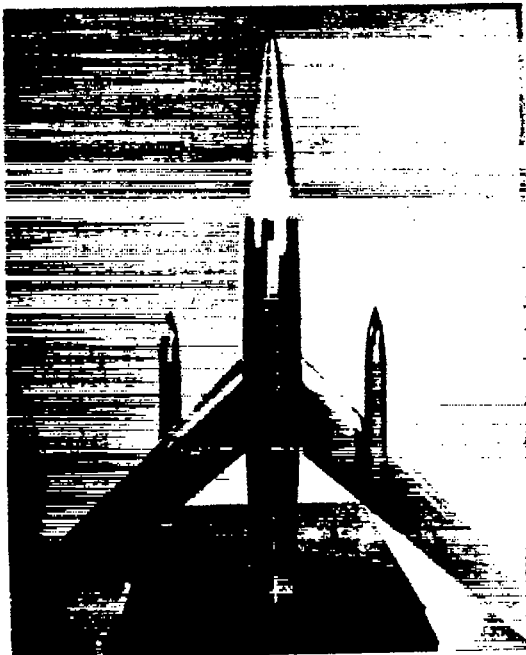
Model G, $\frac{e}{c} = 0.35$.

(b) Models with symmetrically mounted nacelles.

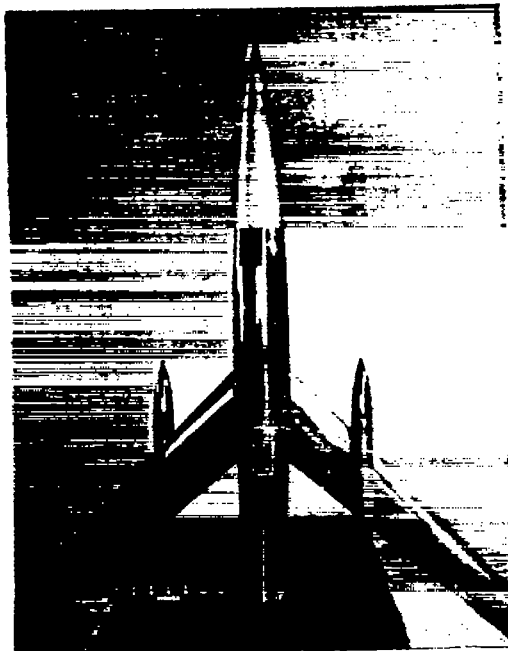
NACA
L-64913

Figure 3.- Continued.

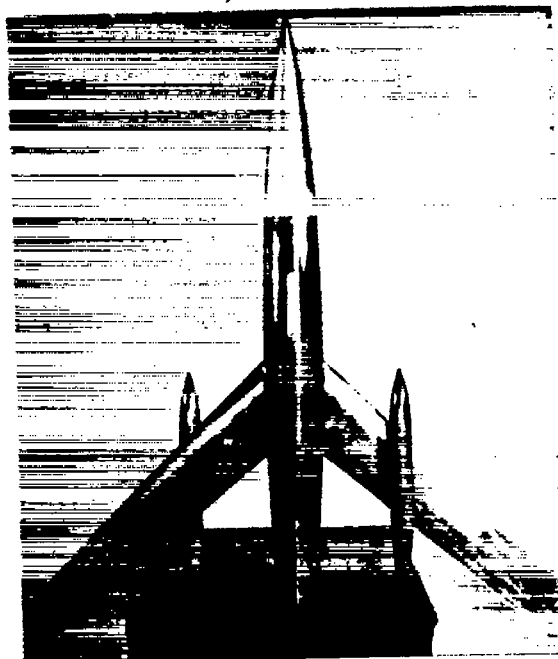




Model H, $\frac{e}{c} = 1.20$.



Model J, $\frac{e}{c} = 0.76$.



Model K, $\frac{e}{c} = 0.50$.

(c) Models with underslung nacelles.

Figure 3.- Concluded.

NACA
L-64914

[REDACTED]

[REDACTED]

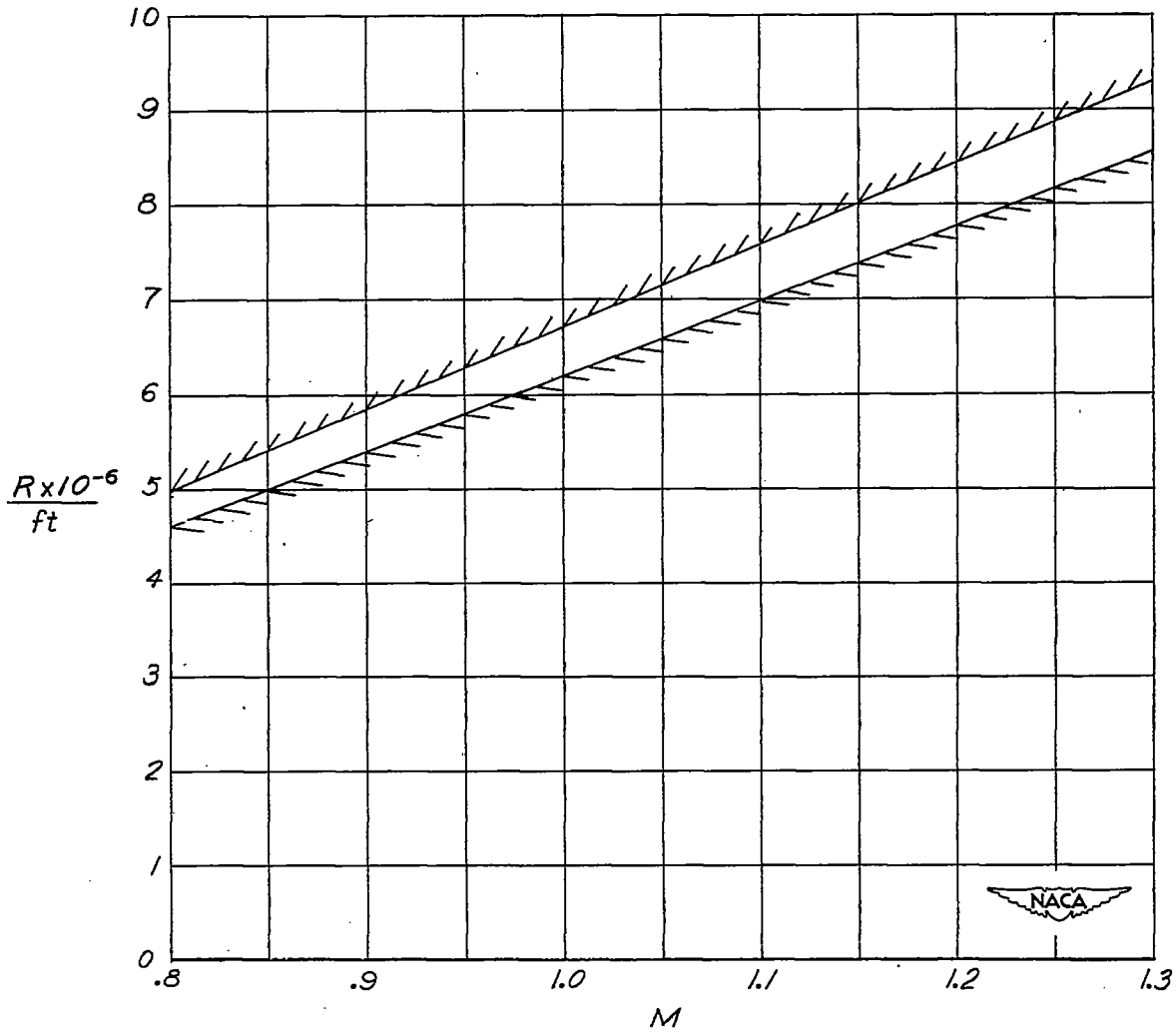


Figure 4.- Variation of Reynolds number range with Mach number for models tested.

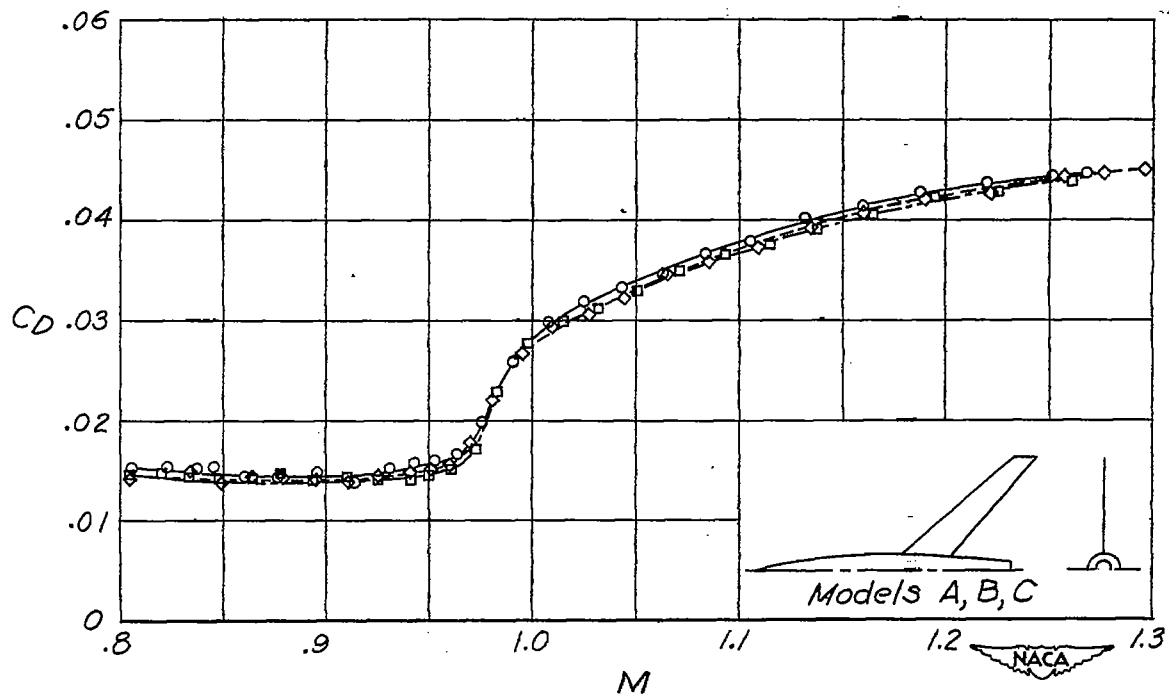
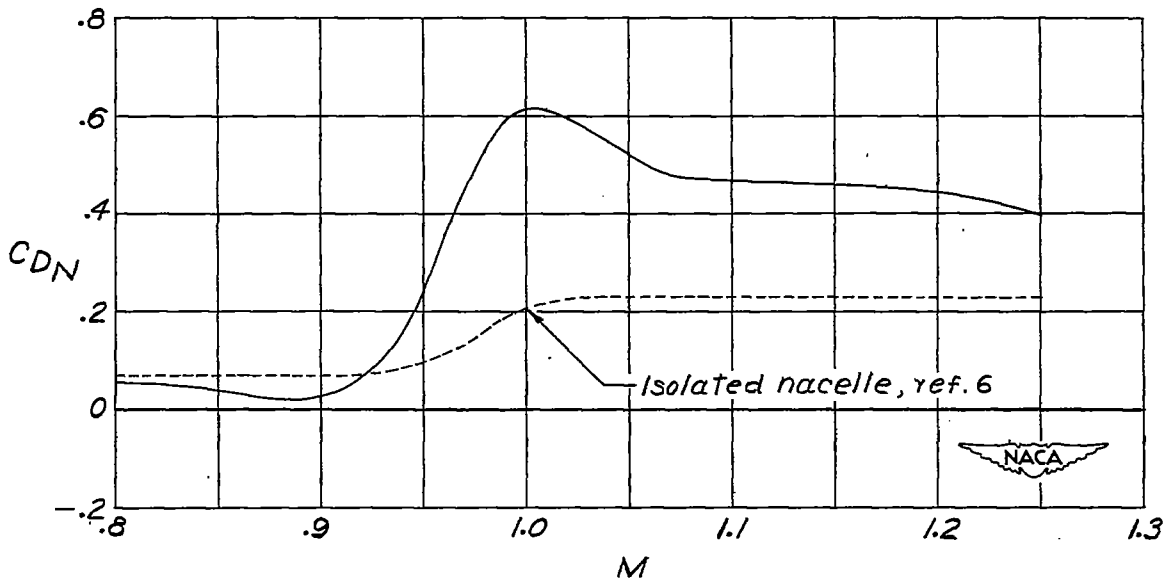
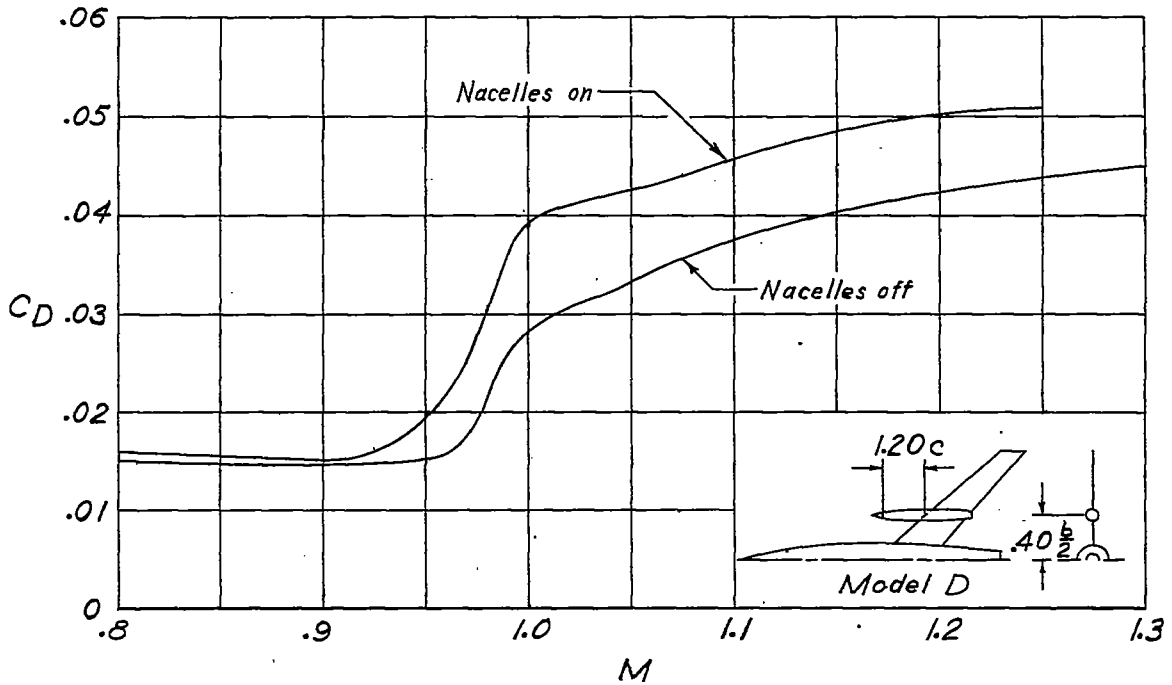


Figure 5.- Variation of drag coefficient for models without nacelles.



(a) Symmetrically mounted nacelles at $1.20c$.

Figure 6.- Variations of total drag, wing-body drag, and nacelle drag coefficients with Mach number for nacelles located at 40 percent of the wing semispan.

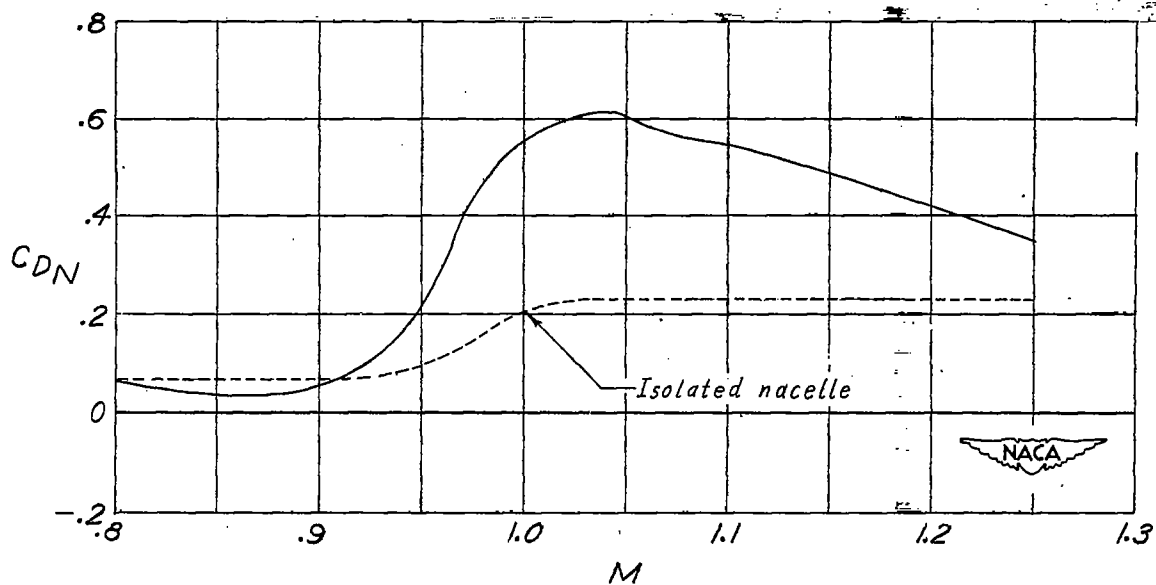
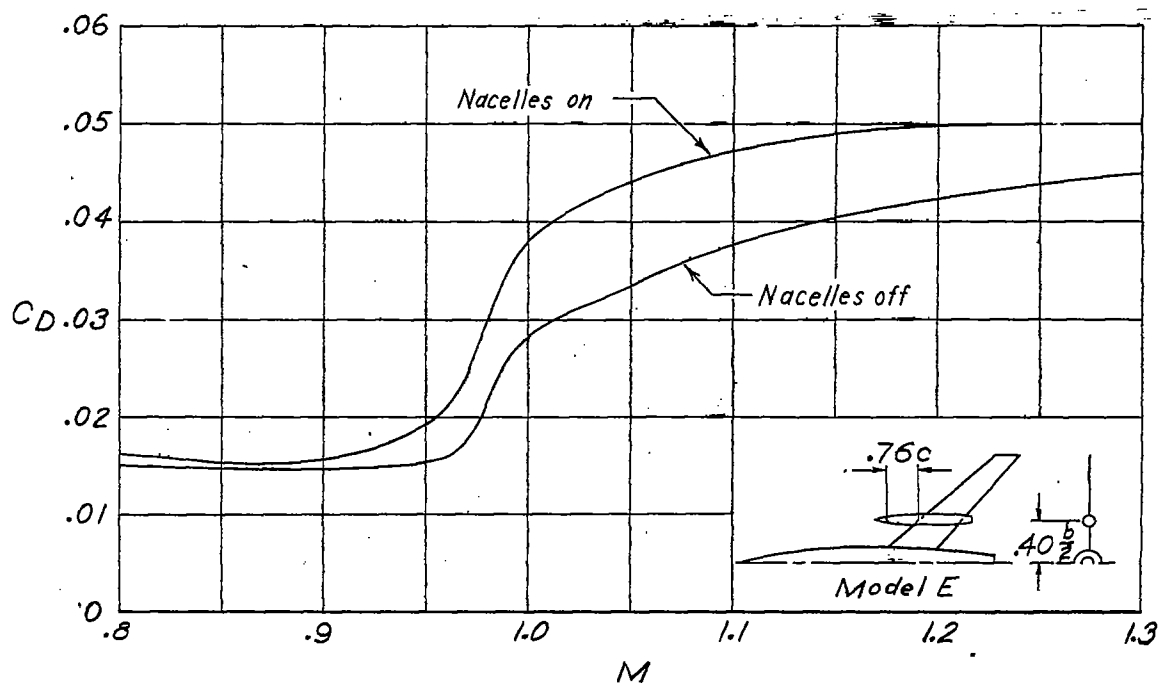
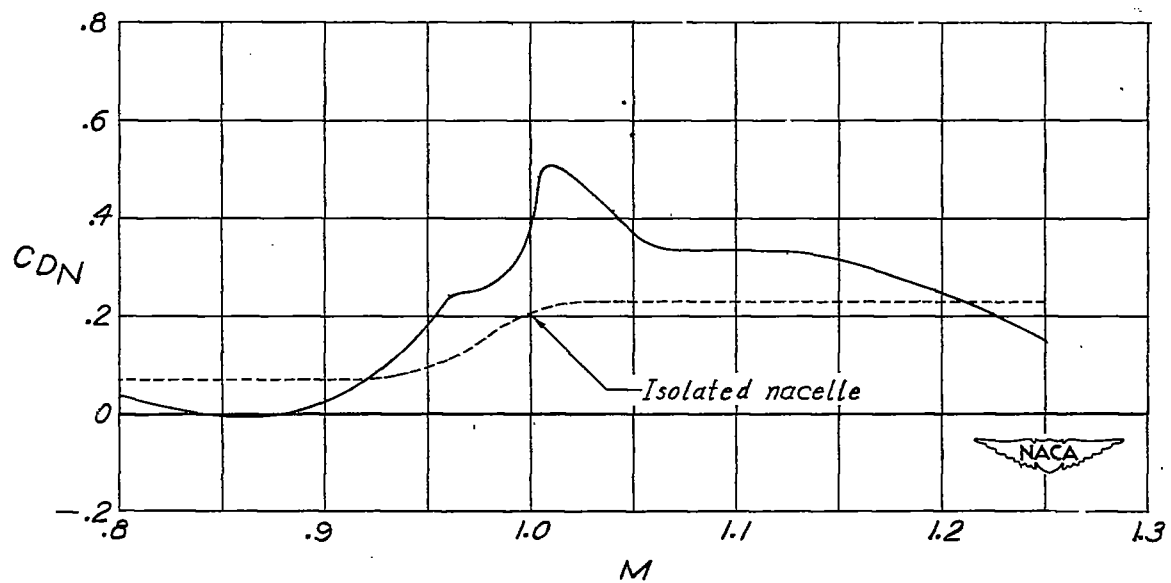
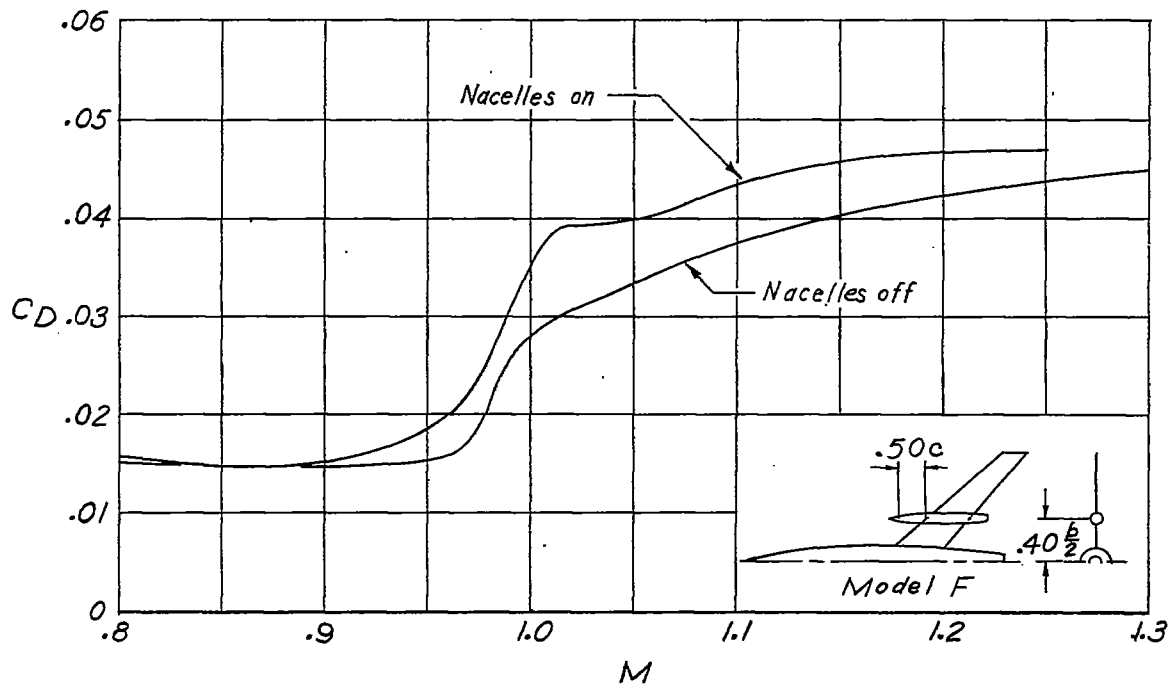
(b) Symmetrically mounted nacelles at $0.76c$.

Figure 6.- Continued.



(c) Symmetrically mounted nacelles at 0.50c.

Figure 6.- Continued.

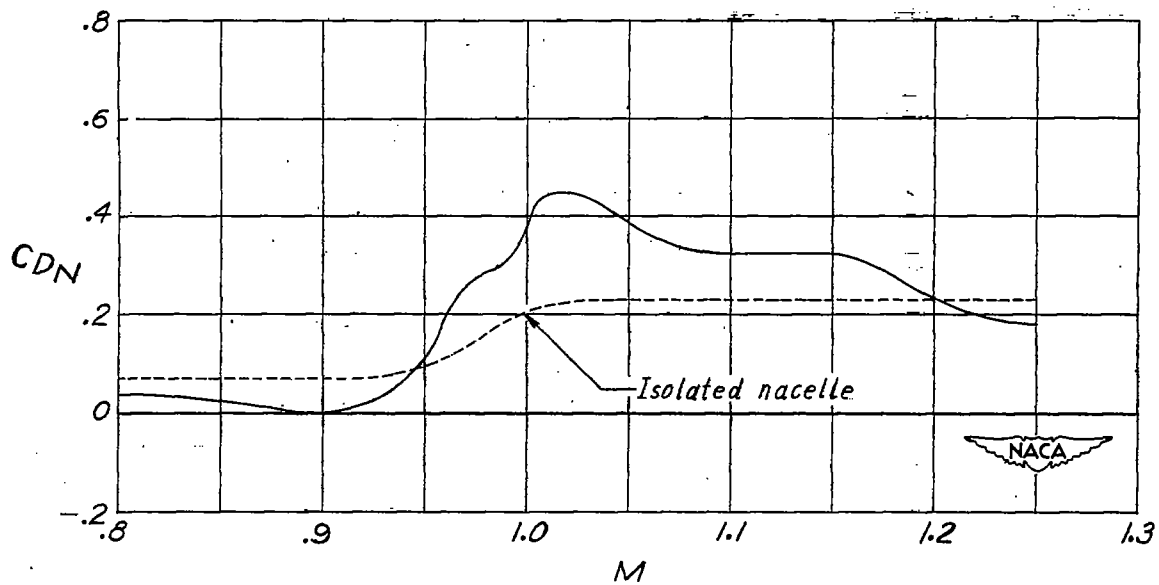
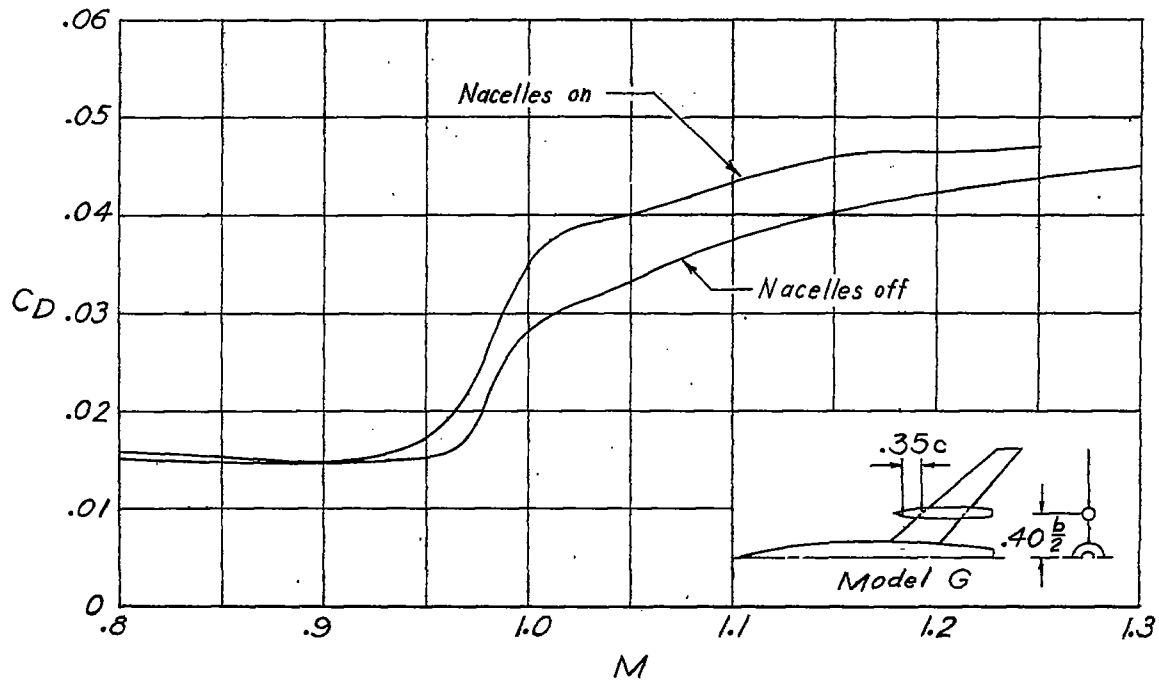
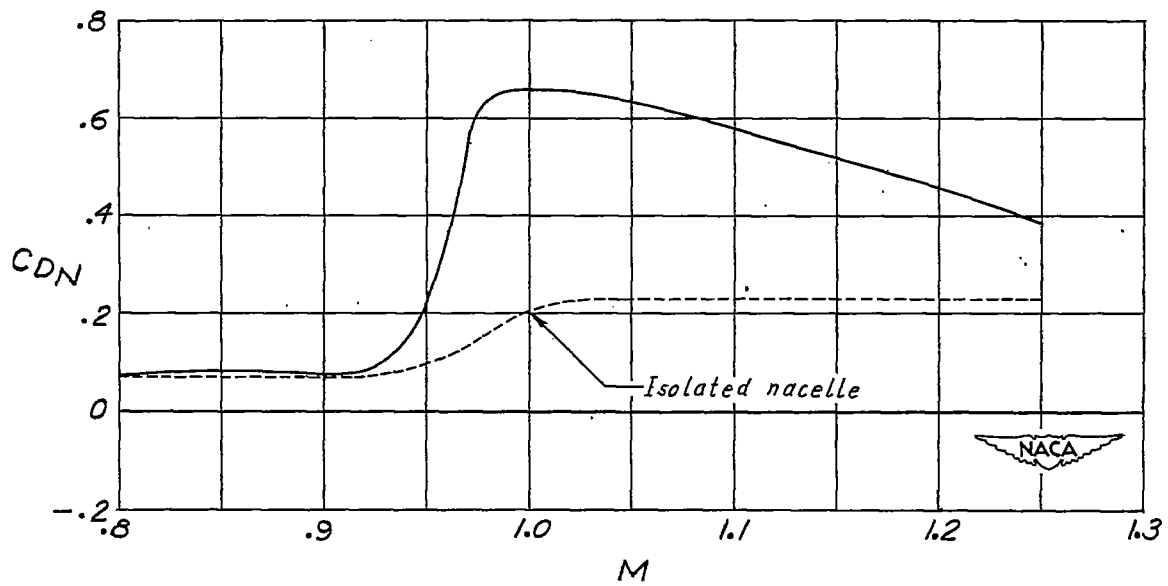
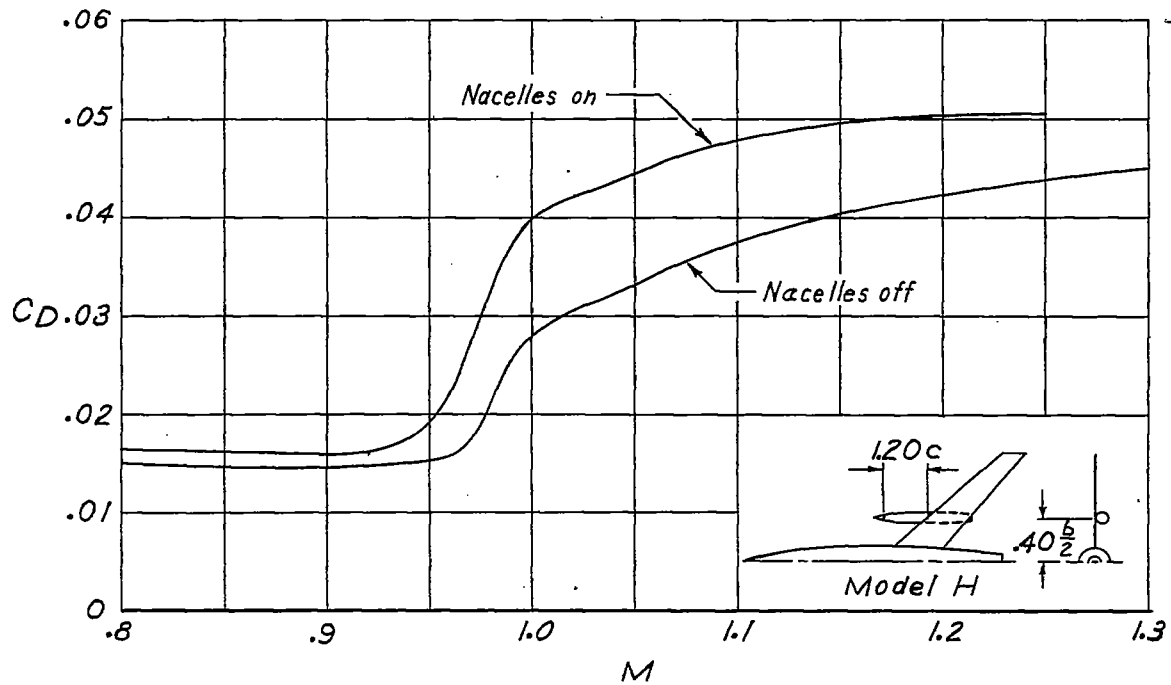
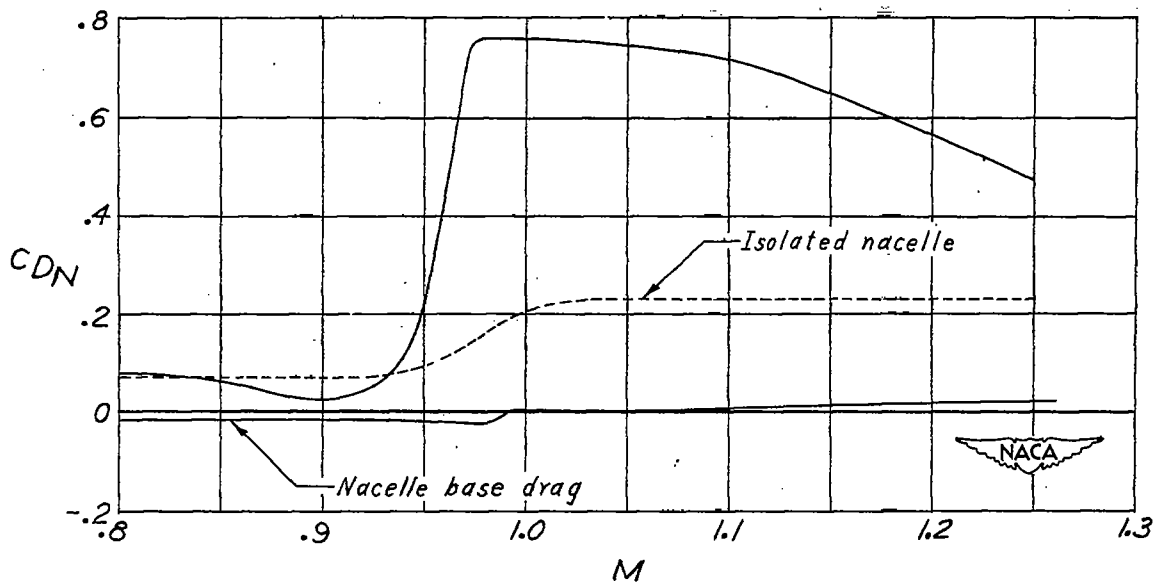
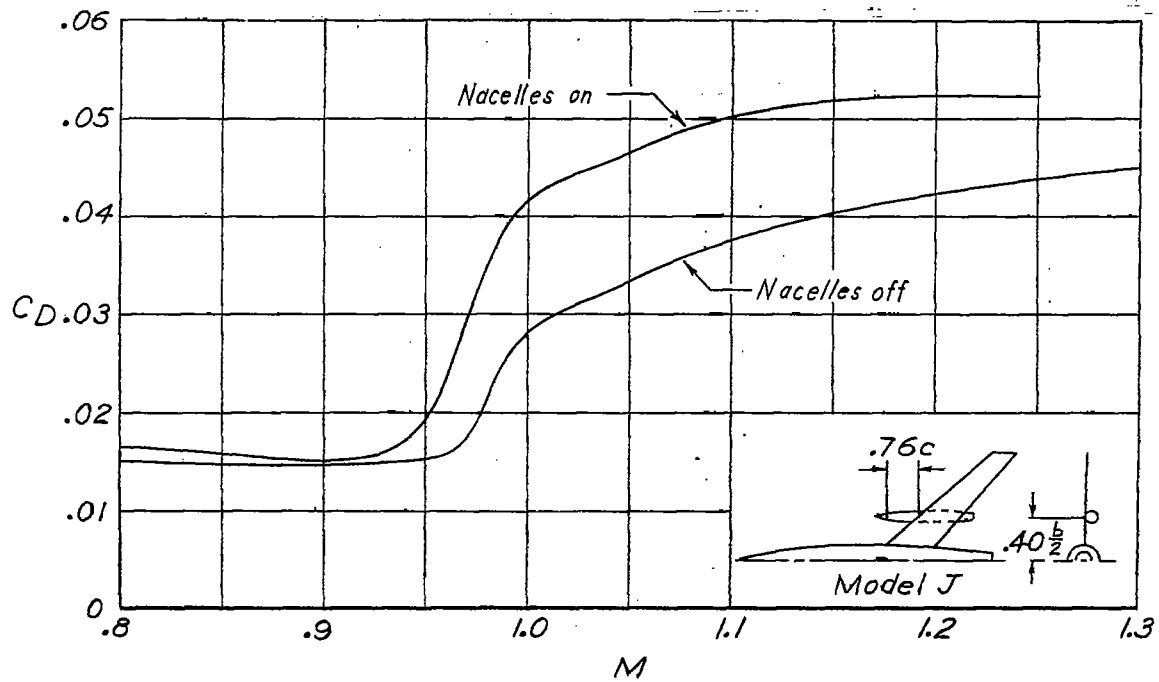
(d) Symmetrically mounted nacelles at $0.35c$.

Figure 6.- Continued.



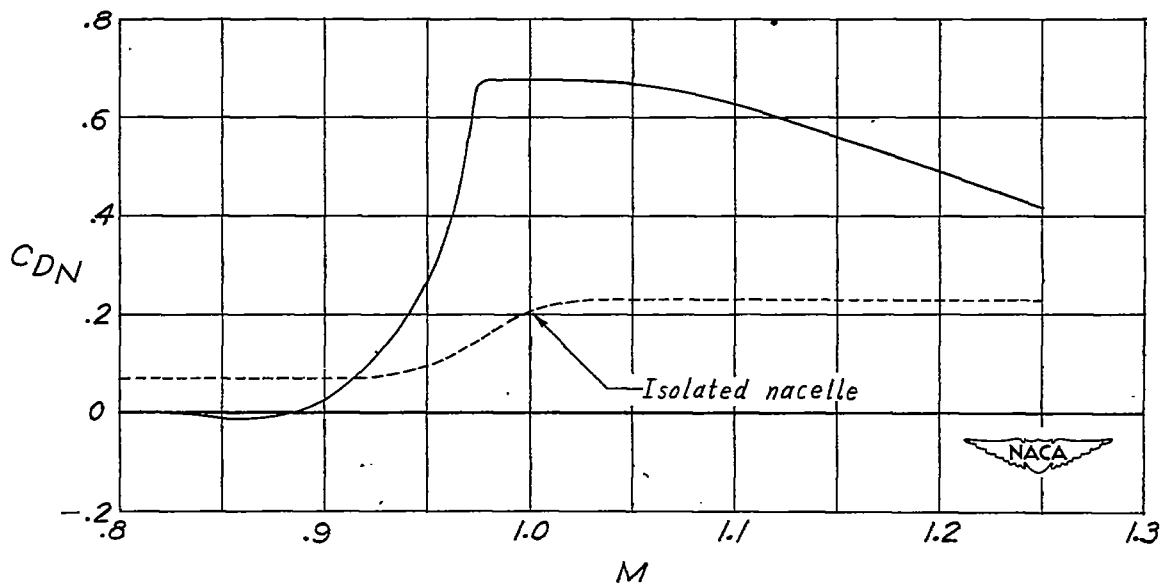
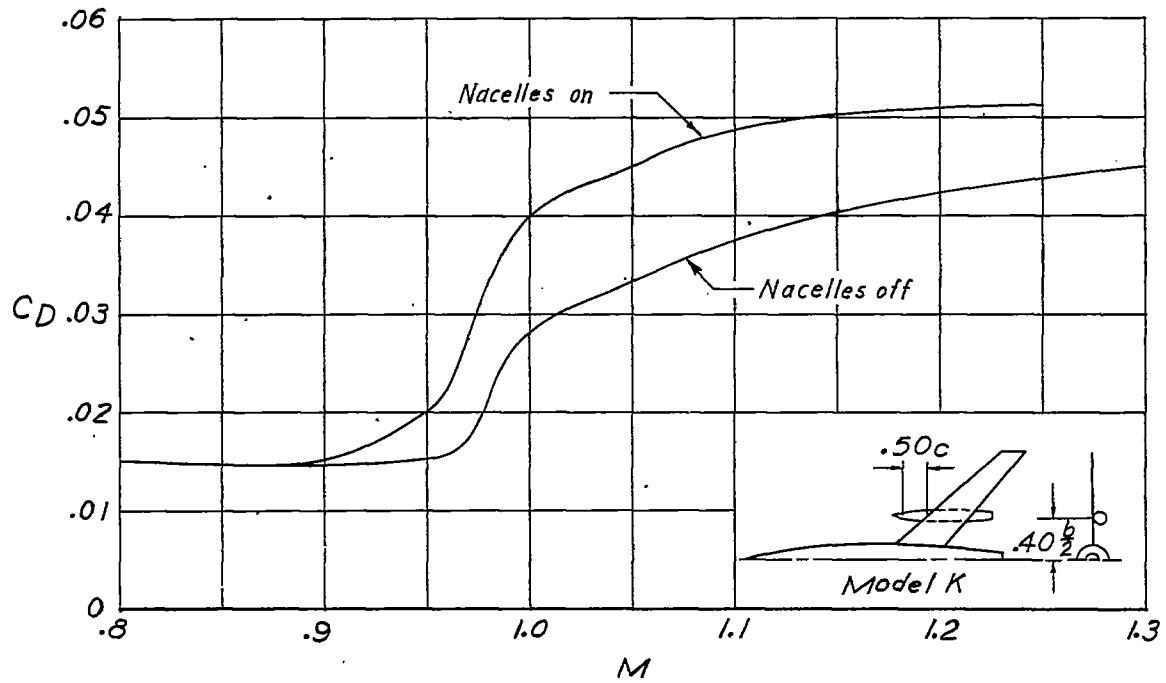
(e) Underslung nacelles at 1.20c.

Figure 6.- Continued.



(f) Underslung nacelles at 0.76c.

Figure 6.- Continued.



(g) Underslung nacelles at 0.50c.

Figure 6.- Concluded.

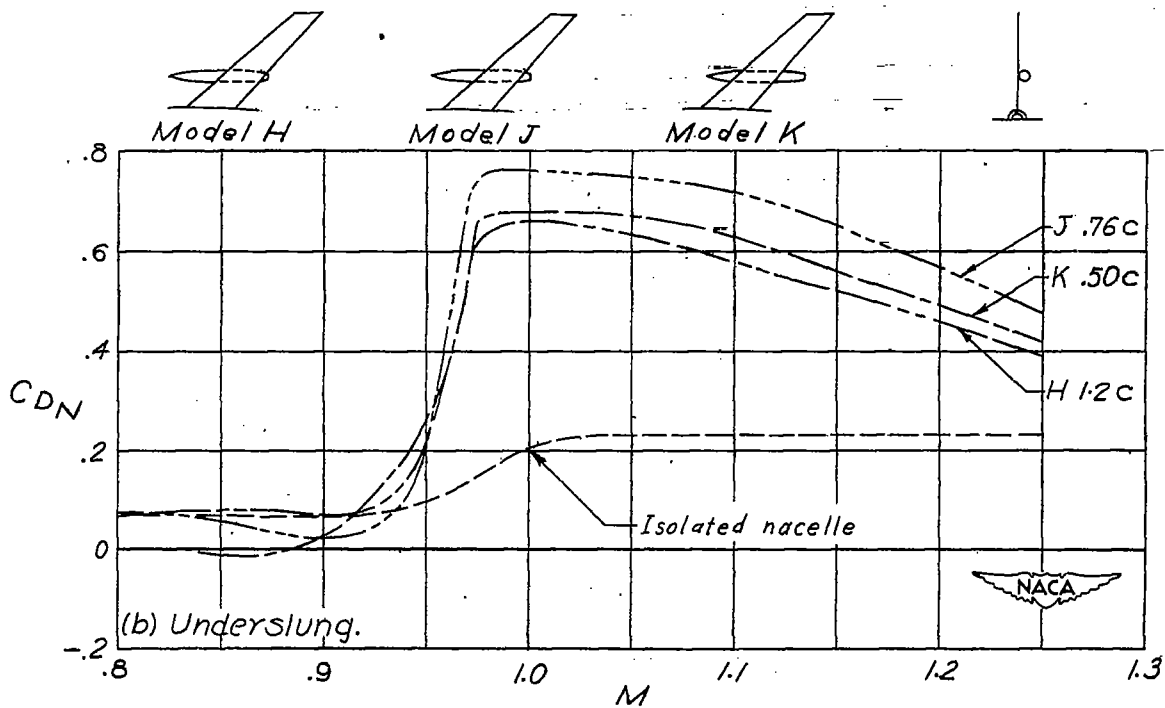
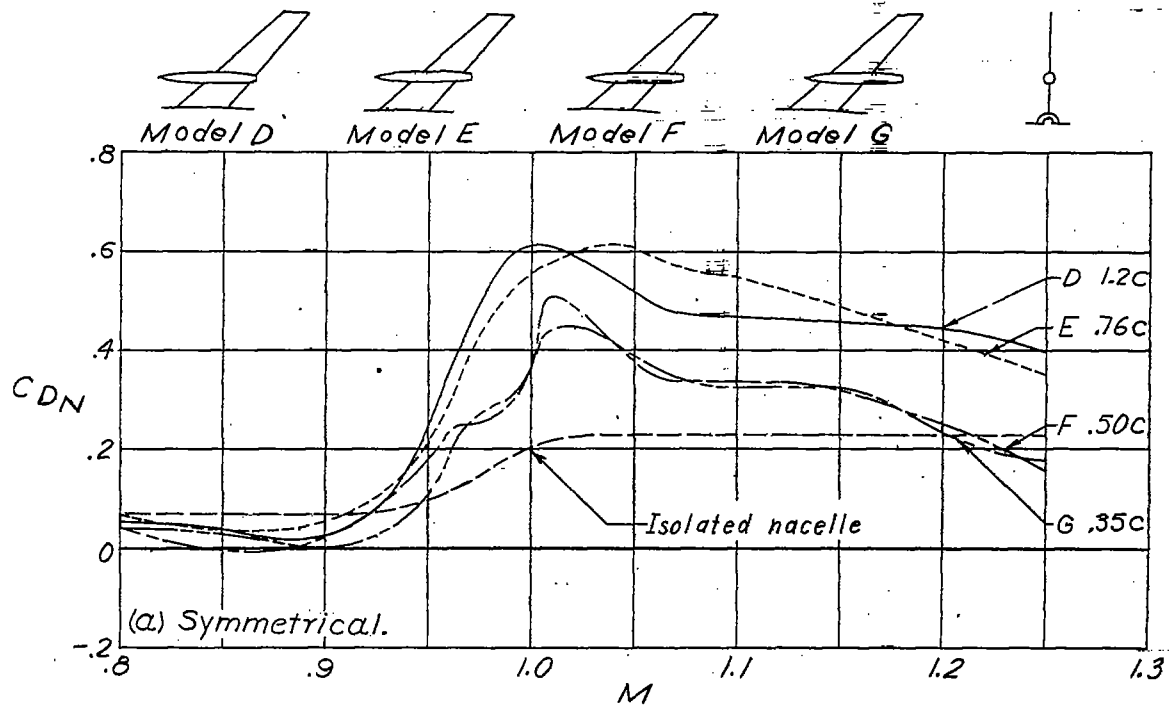


Figure 7.- Variations of nacelle drag coefficients with Mach number for nacelles mounted in various chordwise locations and in symmetrical and underslung positions.

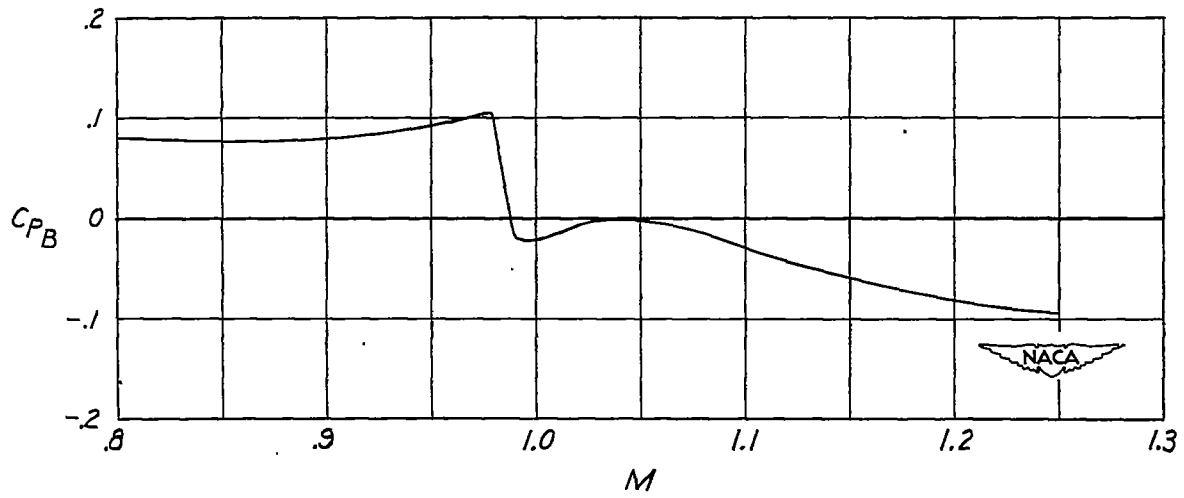


Figure 8.- Variation of nacelle base-pressure coefficient with Mach number for model J.

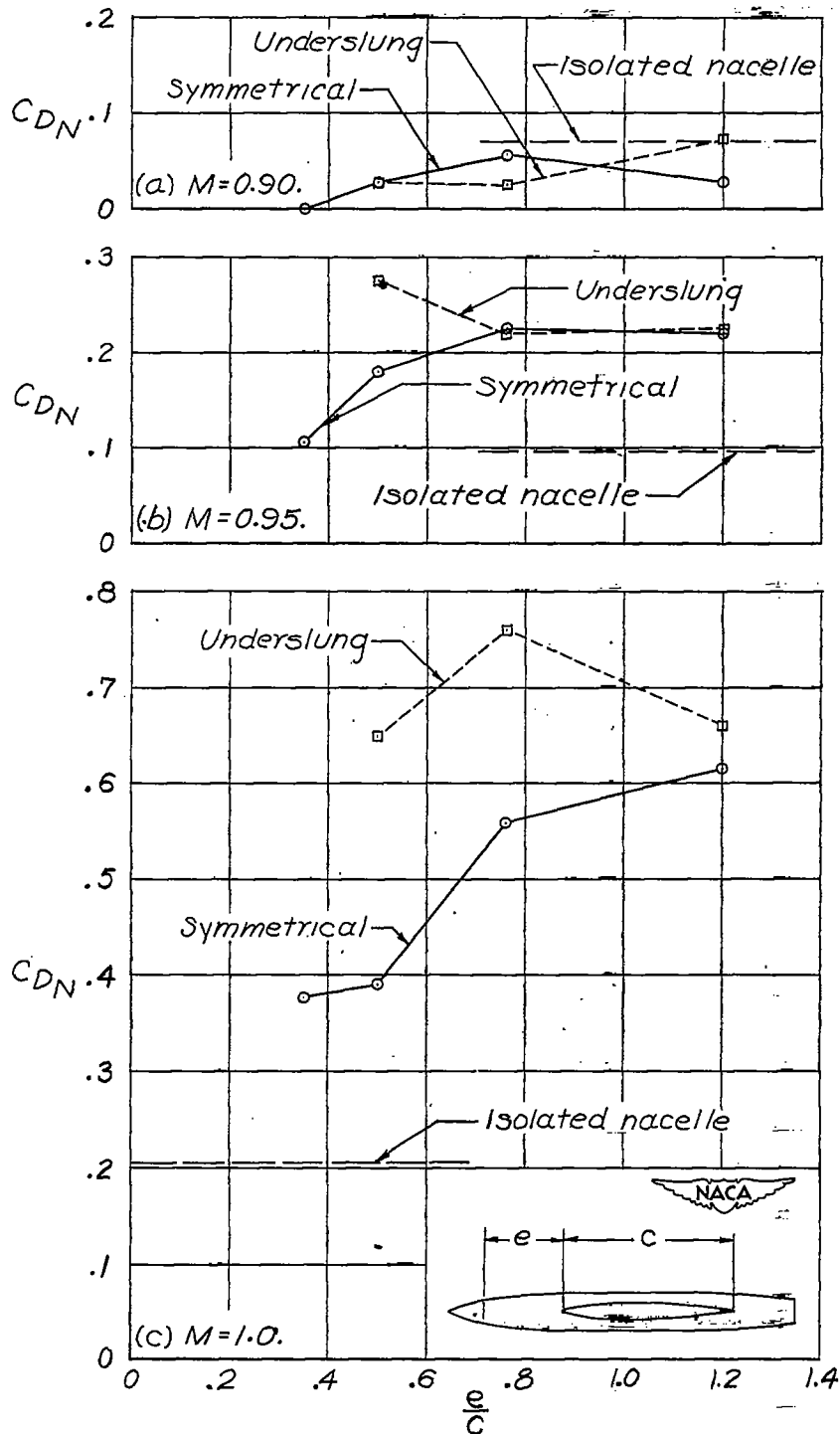


Figure 9.- Variations of nacelle drag coefficient with chordwise location of nacelles in symmetrical and underslung positions for various Mach numbers.

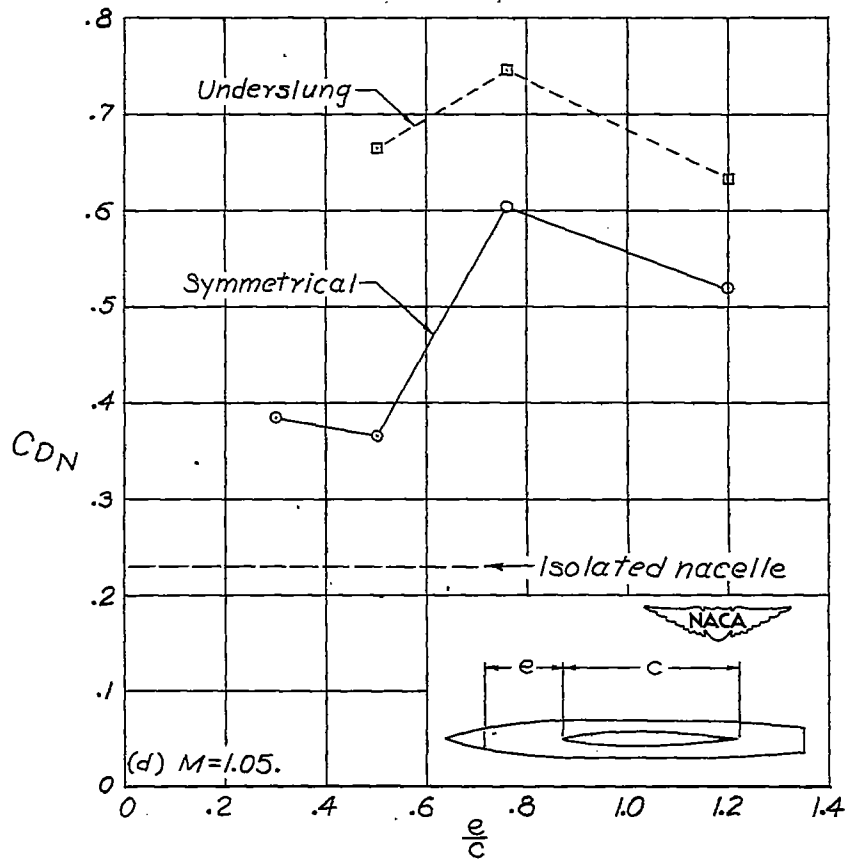


Figure 9.- Continued.

~~CONFIDENTIAL~~

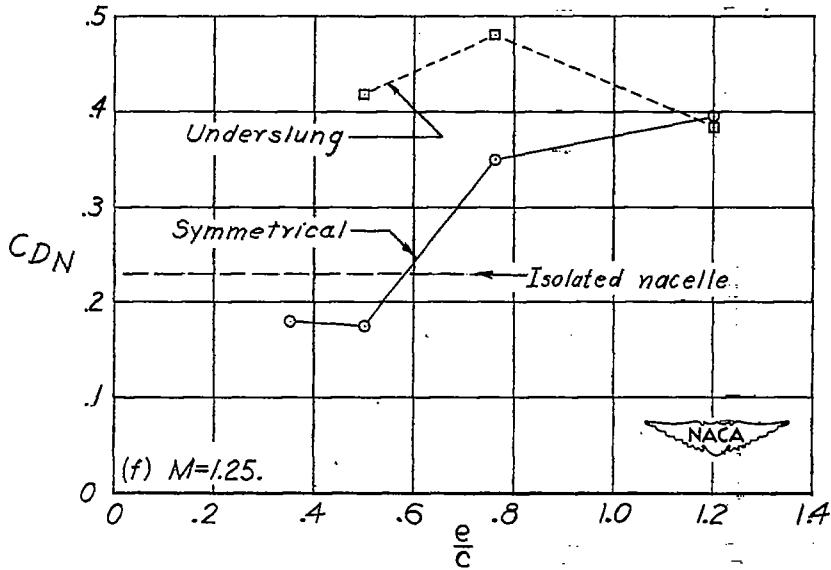
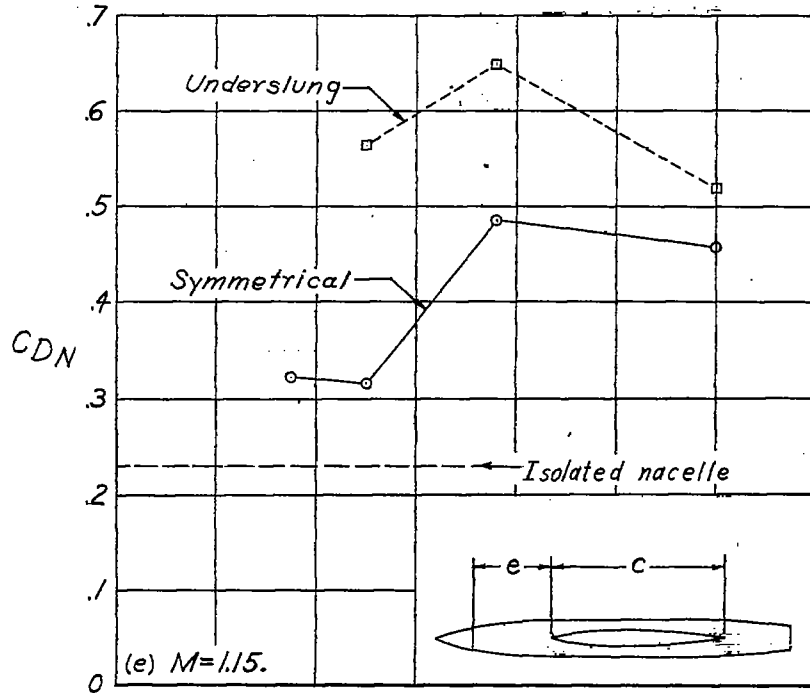


Figure 9.- Concluded.

~~CONFIDENTIAL~~